Influence of alloying and holding time on microstructure and corrosion fatigue behaviour of brazed AISI 304L/NiCrSiB joints

J. L. Otto, A. Schmiedt-Kalenborn, F. Walther*

Department of Materials Test Engineering, TU Dortmund University, Dortmund, Germany

** Corresponding author: johannes.otto@tu-dortmund.de*

M. Penyaz, A. Ivannikov, B. Kalin

Department of Materials Science, National Research Nuclear University, Moscow, Russia

---

Abstract

For numerous industrial applications, such as turbine or heat exchanger constructions, the corrosion fatigue behaviour of vacuum brazed joints is of great interest for the life-time determination. In addition to the influence of the joining geometry, this behaviour depends primarily on the microstructure of the brazed seam. This in turn is largely determined by the alloy composition of the brazing filler metal and the brazing process parameters. Knowledge of the alloy-process-structure-property relationships is therefore essential to improve the corrosion fatigue properties. In this study, vacuum brazed AISI 304L/NiCrSiB cylindrical butt joints were investigated in multiple and constant amplitude tests in a self-developed corrosion measuring cell with application-specified sensors. To investigate the influence of the alloy composition with regard to the chromium and additional molybdenum content, two different amorphous-crystalline rapidly quenched filler metal foils were produced. Using two different holding times at 1160°C during the brazing process, the influence on the formation of borides and silicides was also investigated on the basis of cross sections by scanning electron microscopy. In previous investigations on a filler metal with a 20% Cr and 4% Mo content, a clear homogenization of the brazed seam could be observed for longer holding times, whereby a more ductile material behaviour was achieved, which in turn positively influenced the corrosion fatigue properties. The positive influence of chromium on the corrosion resistance could be demonstrated, but the present study shows that improved corrosion properties due to a higher Cr content are not necessarily accompanied by improved fatigue properties. This could be demonstrated with a Mo-free, 7% Cr filler metal by a fourfold increase in the number of cycles to failure. Finally, fractographic investigations were carried out to characterize the microstructure-dependent damage mechanisms.

1 Materials

1.1 Alloy compositions and brazing process parameters

Pure elemental ingots of Fe, Ni, Cr, Mo and ligatures of Si and B were moulded in an induction furnace to produce the alloys for two different experimental filler metals according to the composition given in *Tab. 1*. In accordance to the industrial Russian grade of foils "STEMET®" [1], they were shortly referred to "ST" followed by their Cr wt.-%. By rapidly solidification of a flat jet melt on a fast-rotating copper disk, foils with a thickness of 45 ± 5 µm were obtained. These filler metal foils were used to braze cylindrical butt joints of AISI 304L. Therefore, rods of these base material were cut into pieces of 80 mm and the surface was grounded to avoid brazing defects.

Tab. 1: Compositions of base material and filler metals, in wt.-%

	Fe	**Ni**	**Cr**	**C**	**Si**	**Mn**	**Mo**	**B**
AISI 304L	bal.	8.03	18.14	0.023	0.30	1.54	0.34	-
ST20	4.0	bal.	**20.0**	-	7.5	-	**4.0**	1.5
ST07	4.0	bal.	**7.0**	-	7.5	-	-	1.5

The melting range of this filler metals was investigated by differential thermal analyses (DTA) and used to determine the temperature characteristics of the brazing process. According to DTA the melting point is 1111 °C for ST07 and 1125 °C for ST20, so a brazing temperature of 1160 °C was chosen to ensure that the whole filler metal changed into liquid solution during the brazing processes, which are described in *Tab. 2*. Two different holding times at the brazing temperature were selected to investigate also the effect of the time-depending diffusions processes of the filler metal elements. A vacuum furnace with resistance heating was used for brazing, providing a vacuum of up to $1.3 \cdot 10^{-3}$Pa.

Tab. 2: Time-temperature curve of the brazing process

	1. step of heating	**1. holding time**	**2. step of heating**	**2. holding time**
Mode 1	20 K/min 0 to 900°C	15 min at 900°C	40 K/min 900 to 1160°C	**15 min** at 1160°C
Mode 2	20 K/min 0 to 900°C	15 min at 900°C	40 K/min 900 to 1160°C	**45 min** at 1160°C

1.2 Microstructure and properties

Cross-sections of the alloying- and holding time depending microstructure formations are shown in *Tab. 3*. It clearly shows that a longer holding time increases the thickness of the brazed seam, since the elements have more time to diffuse. The dark spots on the

grain boundaries of the base material show borides. Since boron has the highest diffusion speed due to its small atomic radius, it can diffuse most deeply into the base material and form chromium borides by removing chromium from the surrounding grains. The presence of these borides marks the so-called diffusion zone. But it can be observed that in combination with molybdenum the high chromium content of ST20, especially in the case of the short holding time ($ST20_{15min}$), also leads to a formation of large borides already in the centre and thus to less diffusion into the base material. These brighter zone in the middle of the seam can be divided into the isothermal solidification zone and the athermal solidification zone. The latter is formed from the remaining liquid and can only be observed at ST20. Besides the large borides, these can be the large white phases, which are more complex silicide compounds, as already shown in [2].

Tab. 3: Microstructure of the different brazing seams in SEM with BSE detector

	15 min holding time	**40 min holding time**
ST20	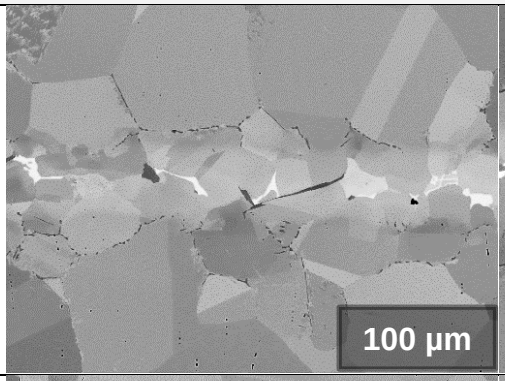	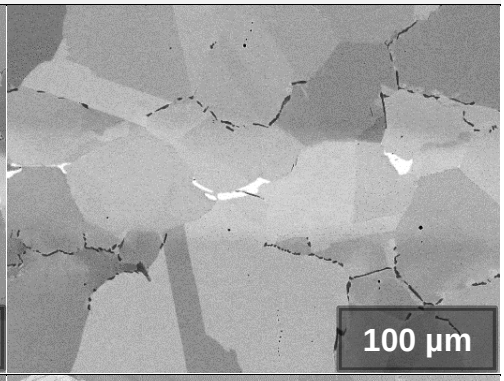
ST07	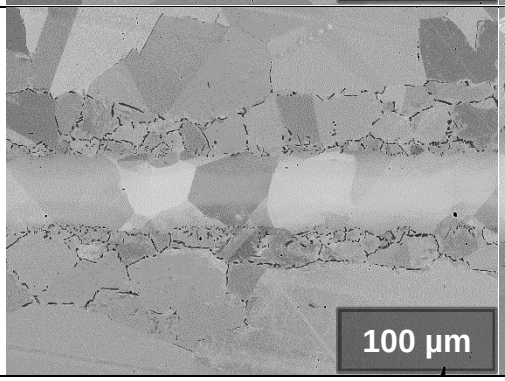	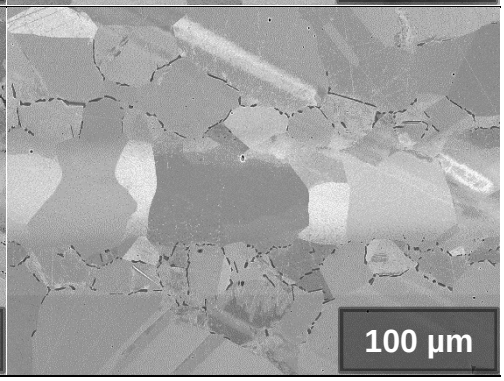

The amount, size and distribution of the borides and other brittle phases are also reflected in the Vickers micro-hardness values ($HV_{0.1}$), which are shown in *Tab. 4*. For a more specific determination, nanoindentation should be used [3], but the gradient of these large-area hardness values through the brazed seam gives information about the mechanical properties. The most uniform gradient was observed for $ST07_{40min}$.

Tab. 4: Vickers micro-hardness investigation of brazed joints

		ST07$_{15min}$	**ST07$_{40min}$**	**ST20$_{15min}$**	**ST20$_{40min}$**
Base material	[$HV_{0.1}$]	174	167	173	168
Diffusion zone	[$HV_{0.1}$]	249	183	191	180
Isothermal solidification zone	[$HV_{0.1}$]	169	167	233	161
Athermal solidification zone	[$HV_{0.1}$]	-	-	365	367

The corrosive resistance of the different microstructures is important to understand the corrosive effect of the corrosion fatigue results. These were determined in [4] where a detailed description of the methods is given. The results are shown in *Tab. 5*. The corrosion depth was measured on cross-sections after boiling the specimens in a solution of 5 wt.-% $CuSO_4$ and 25 vol.-% H_2SO_4 at 110°C for 8 hours. Also, a corrosion rate was determined by potential dynamic polarization of the cylindrical specimens in K2.2, which correlate with the depth of corrosion. The ST20 alloy showed due to their high Cr-content the highest corrosion resistance, since there is enough chromium to avoid a significant locally chromium depletion due to the chromium boride formation.

Tab. 5: Corrosion resistance determined in [4]

		ST07$_{15min}$	**ST07$_{40min}$**	**ST20$_{15min}$**	**ST20$_{40min}$**
Corrosion depth *	[µm]	90	27	14	3
Corrosion rate	[mg a^{-1} cm^{-2}]	4.41	1.69	1.33	0.74

* The error is ± 5 µm

2 Experimental setup and procedure

The corrosion fatigue tests were performed with a servo-hydraulic testing-system (Instron, 8801, F = ± 100 kN) and a self-developed corrosion cell, which is continuously flown through by synthetic exhaust gas condensate K2.2 according to VDA-230-214 [5] tempered to 22°C. The whole setup is shown in *Fig. 1*. Two extensometers were used to measure the strain. One inside the corrosion cell with an initial gauge length of L_0 = 5 mm to measure the strain in the region of interest as locally as possible, but which cannot completely measure the strain due the high ductility, and one outside the measuring cell with an initial gauge length of L_0 = 63 mm, which can measure the strain completely. Besides the strain measurement a three-electrode system with an Ag/AgCl-reference electrode to measure the electrochemical open circuit potential (E_{OCP}) was used. This value indicates the breakdown and repassivation of the passive layer due to the strain-induced formation of in- and extrusions [6]. But mostly it reacts to the crack

opening, since the rapid exposure of the inner material, which has not yet been able to form a passive layer, generates corrosion products much faster, which increase the conductivity of the corrosion medium.

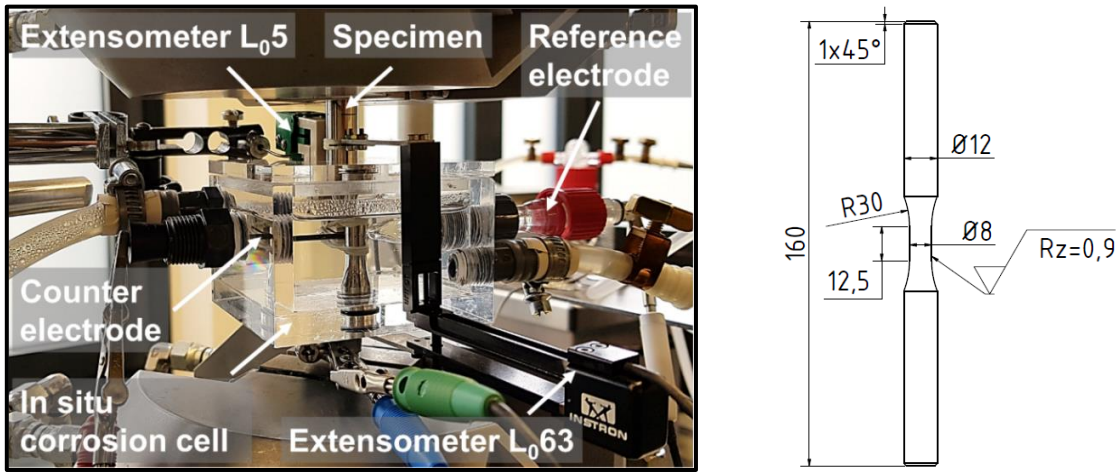

Fig. 1: Corrosion fatigue test setup [2] and fatigue specimen geometry

All tests were carried out at a frequency f = 10 Hz and a stress ratio R = 0.1 (tension-tension region). Multiple amplitude tests were carried out starting from the maximum stress $\sigma_{max,start}$ = 50 MPa with a stepwise increase of $\Delta\sigma_{max}$ = 5 MPa after each $\Delta N = 10^4$ cycles until specimen failure.

3 Results and discussion

3.1 Multiple amplitude tests

In *Fig. 2* a multiple amplitude test of $ST07_{40min}$ is shown, which reached 390 MPa after $68.2 \cdot 10^4$ cycles. This was the best result that could be observed for all four variations.

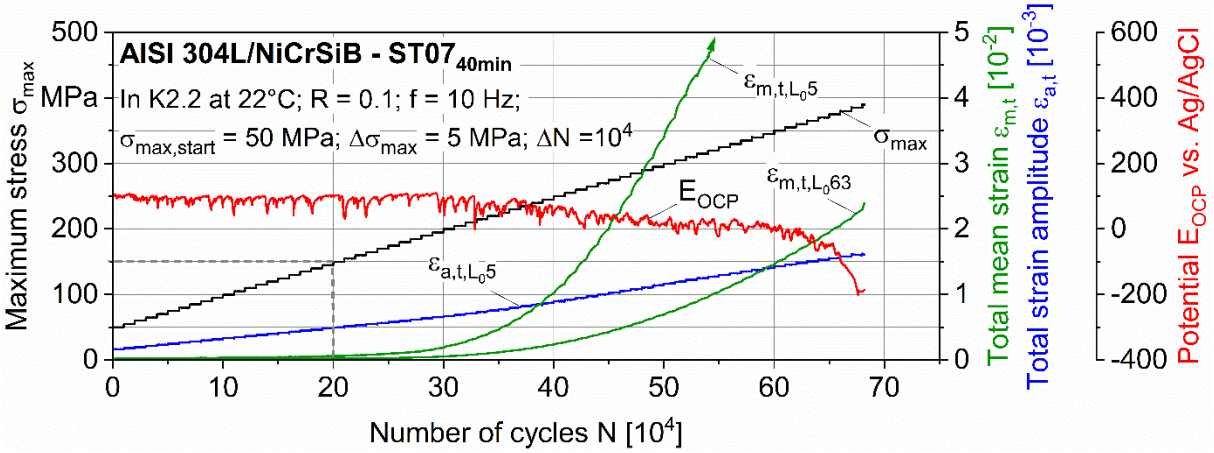

Fig. 2: Corrosion fatigue behaviour of $ST07_{40min}$ during multiple amplitude test

For comparison: $ST20_{40min}$ failed at 280 MPa after $46.2 \cdot 10^4$ cycles. It could be found out, that a longer holding time increases the ductility. So the first significant reaction of the total mean strain $\varepsilon_{m,t}$ (marked with grey dashed lines), which indicates the starting plastic deformation, was for both 40 min variations at 150 MPa but for the 15 min variations at about 190 MPa. Since the longer holding time was most promising, only these were used in the following tests.

3.2 Constant amplitude tests

Additionally, constant amplitude tests were carried out at different stress amplitudes as shown in *Fig. 3* for $ST07_{40min}$ at 300 MPa. Due to the rapid increase of stress at test beginning, the E_{OCP} initially drops and then restores the original state in a phase of repassivation, which is interrupted by in- and extrusion formation. However, the first microcracks and finally macrocracks lead to a stronger decrease of the E_{OCP}.

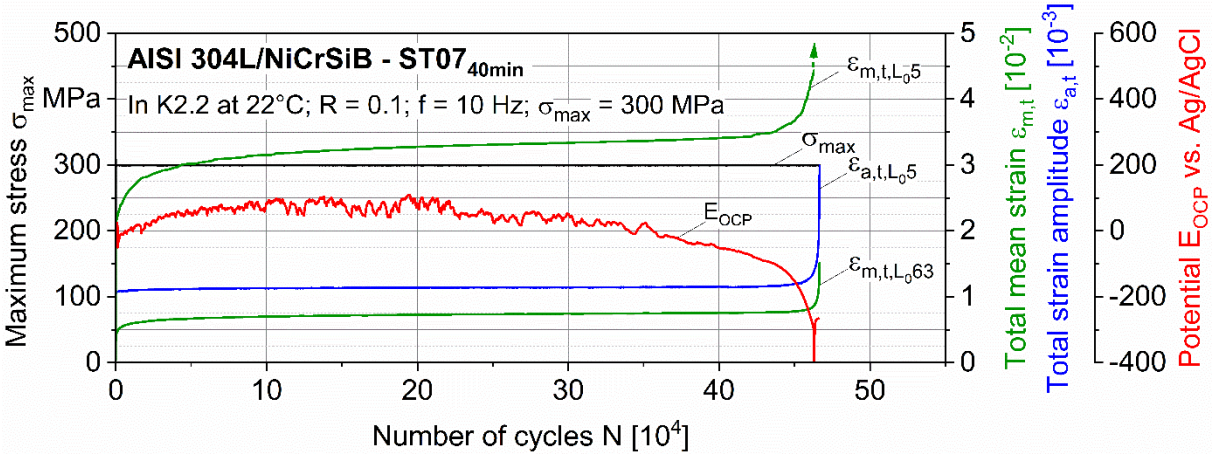

Fig. 3: Corrosion fatigue behaviour of $ST07_{40min}$ during constant amplitude test at 300 MPa

Fig. 4 shows the results of the constant amplitude tests in form of the Woehler (S-N) curve. Results that differ significantly from the estimated course are often due to brazing defects at the edge of the seam, which led to crack initiation. These defects only become visible through fractographic investigations and show unwetted areas with diameters of up to 100 µm.

$ST20_{40min}$ shows a similar curve at higher stress level as shown in [7], [8] for the industrial filler metal BNi-2, with the difference that from $2 \cdot 10^5$ cycles on the slope drops only half as steeply. This difference is most likely due to the high corrosion resistance as given in *Tab. 5*. A special effect was observed for the $ST07_{40min}$ specimens, which leads to a significant change in the S-N curve: from 360 MPa on these specimens did

not fail anymore in the brazing seam. Already from 320 MPa on, cracks appear in several places, which is shown in *Fig. 5*, and for the tests at 380 and 400 MPa, the final crack propagation took place at a significant distance from the brazing seam (distance > 3 mm). It seems that the effect of borides or brazing defects become less important at these high stress amplitudes, to the point where they are no longer a cause of failure. Another cause of failure in the base material can be stress-induced martensite formation, which is more sensitive to stress corrosion cracking [8], [9].

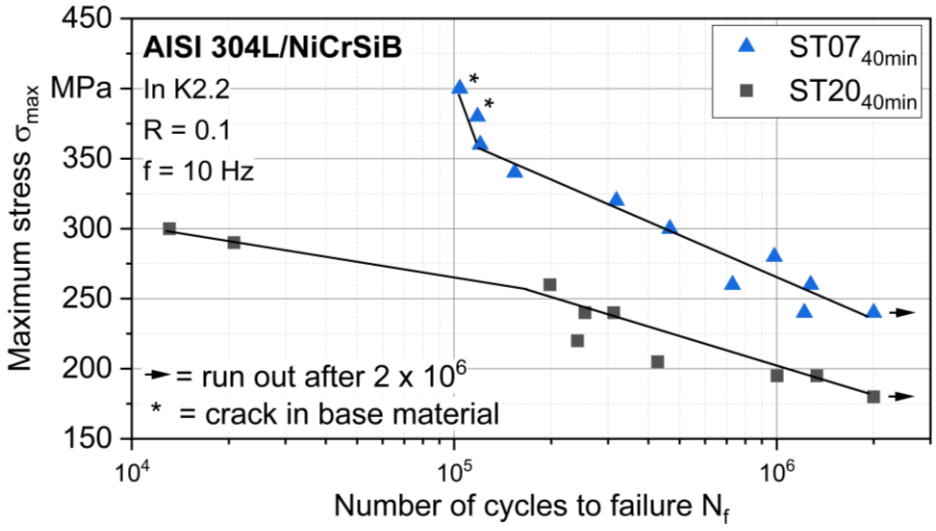

Fig. 4: S-N curves for ST07$_{40min}$ and ST20$_{40min}$

Since corrosion mechanism are time-depending it could be that there is an intersection of the two corrosion fatigue curves in the high cycle fatigue region. Also for lower frequencies, a stronger influence of corrosion can therefore be assumed, so that an intersection point could then be reached earlier. This could also be possible in a more aggressive environment.

3.3 Fractography

As an example for the fracture behaviour, *Fig. 5* shows a ST07$_{40min}$ specimen that failed in a constant amplitude test at 320 MPa. Two crack initiation areas are clearly visible. The area marked as "I" is the fatigue fracture area, where at high magnification, intragranular splitting is visible. The relief details can be caused by splitting along the microtwins due to plastic deformation, or they are fusions of the main crack with minor cracks. Area "II" is the more rapidly developed forced fracture area, which can also be referred to an intragranular pitting fracture. It is caused by the fusion of micropores, which are formed at the interface between the base metal and borides. The fracture progression thus took place in the diffusion zone, with jumps in the crack progression visible due to the topography.

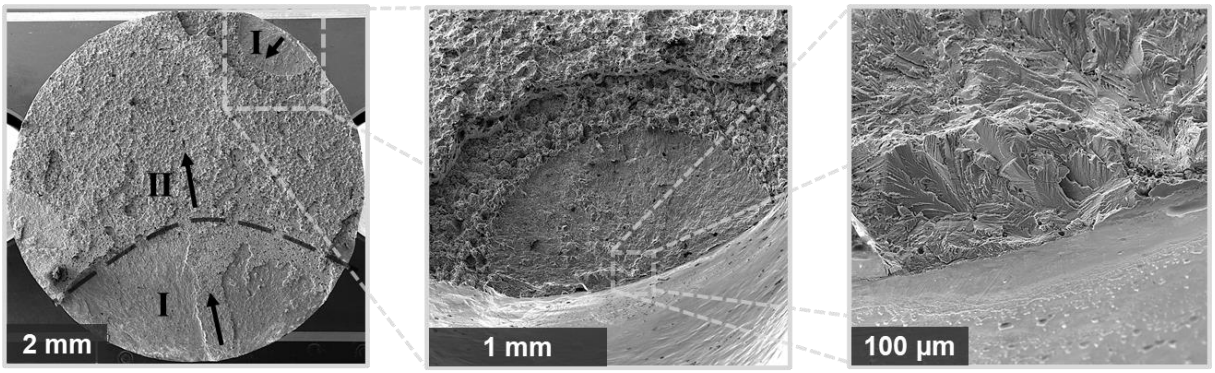

Fig. 5: Fractography of $ST07_{40min}$ failed at 320 MPa after $3.2 \cdot 10^5$ cycles

4 Conclusions and outlook

The influence of alloying and holding time on the microstructure of AISI 304L/NiCrSiB could be investigated and has shown that a high Cr-content in combination with Mo can lead to formation brittle phases like borides, which is even further increased by using a short holding time. Vickers micro-hardness investigations showed the most uniform hardening gradient for a low Cr-, Mo free-alloy brazed with a long holding time. This variation showed the best results in the stress-life curve, despite the lower corrosion resistance. Occurring stress peaks could be reduced by plastic deformation, which led to a significantly higher number of cycles and a significantly higher maximum stress amplitude and for high stress levels it could even be shown, that the ultimate fracture only takes place in the base material.

For further investigations, microstructure based investigations (like electron backscatter diffraction and nanoindentation) from intermittent tests on crack tips and the brazing seam should be performed to explain strengthening mechanisms during cyclic loading to understand the shift of the fracture into the base material. Also tests at lower frequencies and lower stress amplitudes or in a more aggressive corrosion medium at higher temperatures are necessary to further evaluate corrosion effects.

Acknowledgement: The study was funded by the German Research Foundation (Deutsche Forschungsgemeinschaft, DFG) - project No. 408904168 and the Russian Foundation for Basic Research (RFBR) - project No. 19-52-12030 with the title “Alloying-dependent microstructure influence on corrosion fatigue mechanisms of brazed AISI 304/NiCrSiB joints”.

References

[1] Sevryukov, O. N.; Suchkov, A. N.; Guseva, E. V.: Brazing of modern engineering materials with STEMET® amorphous brazing filler metals. Non-Ferrous Met. 1 (2015) p. 45-49.

[2] Otto, J. L.; Penyaz, M.; Schmiedt-Kalenborn, A.; Knyazeva, M.; Ivannikov, A.; Kalin, B.; Walther, F.: Effect of phase formation due to holding time of vacuum brazed AISI 304L/NiCrSiB joints on corrosion fatigue properties. J. Mater. Res. Technol. 9 (2020) 5, p. 10550-10558.

[3] Bobzin, K.; Tillmann, W.: Systematic investigation of the properties of brazed joints with application relevant testing procedures II. Düsseldorf: DVS Forschungsvereinigung; 2012. Issue 213.

[4] Penyaz, M.; Otto, J. L.; Popov, N.; Ivannikov, A.; Schmiedt-Kalenborn, A.; Walther, F.; Kalin, B.: Microstructure influence on corrosion resistance of brazed AISI 304 L/NiCrSiB joints. J. Met. Mater. Int. (2021) [Accepted for publication].

[5] VDA recommendation 230-214: resistance of metallic materials to condensate corrosion in exhaust-gas-carrying components; 2018. Berlin, Germany.

[6] Nazarov, A.; Vivier, V.; Vucko, F.; Thierry, D.: Effect of tensile stress on the passivity breakdown and repassivation of AISI 304 stainless steel: a scanninig Kelvin probe and scanning electrochemical microscopy study. J. Electrochem. Soc. 166 (2019) 11, p. 3207-3219.

[7] Schmiedt-Kalenborn, A.; Lingnau, A. L.; Manka, M.; Tillmann, W.; Walther, F.: Fatigue and corrosion fatigue behaviour of brazed stainless steel joints AISI 304L/ BAu-4 in synthetic exhaust gas condensate. Materials 12 (2019) 7, p. 1040-1054.

[8] Schmiedt-Kalenborn, A.: Microstructure-based assessment of fatigue and corrosion fatigue behavior of brazed AISI 304L stainless steel joints using nickel- and gold-based brazing alloys. Dissertation, Technische Universität Dortmund, 2020.

[9] Lebana, M. B.; Tisu, R.: The effect of TiN inclusions and deformation-induced martensite on the corrosion properties of AISI 321 stainless steel. Eng. Failure Analysis 33 (2013), p. 430 – 438.

Author's address

Johannes L. Otto

TU Dortmund University

Department of Materials Test Engineering (WPT)

Baroper Str. 303

D-44227 Dortmund

Phone: +49 231 755 8536

Fax: +49 231 755 8029

Email: johannes.otto@tu-dortmund.de